

# Evaluation of relative transmitted dose for a step and shoot head and neck intensity modulated radiation therapy using a scanning liquid ionization chamber electronic portal imaging device

Mohammad Mohammadi<sup>1,2,3</sup>, Eva Bezak<sup>1,2</sup>

<sup>1</sup>School of Chemistry and Physics, University of Adelaide, <sup>2</sup>Department of Medical Physics, Royal Adelaide Hospital, Adelaide, SA 5000, Australia, <sup>3</sup>Department of Medical Physics, Hamadan University of Medical Sciences, Hamadan, Iran

Received on: 06.04.11

Review completed on: 29.09.11

Accepted on: 06.10.11

## ABSTRACT

The dose delivery verification for a head and neck static intensity modulated radiation therapy (IMRT) case using a scanning liquid ionization chamber electronic portal imaging device (SLIC-EPID) was investigated. Acquired electronic portal images were firstly converted into transmitted dose maps using an in-house developed method. The dose distributions were then compared with those calculated in a virtual EPID using the Pinnacle<sup>3</sup> treatment planning system (TPS). Using gamma evaluation with the  $\Delta D_{max}$  and DTA criteria of 3%/2.54 mm, an excellent agreement was observed between transmitted dose measured using SLIC-EPID and that calculated by TPS (gamma score approximately 95%) for large MLC fields. In contrast, for several small subfields, due to SLIC-EPID image blurring, significant disagreement was found in the gamma results. Differences between EPID and TPS dose maps were also observed for several parts of the radiation subfields, when the radiation beam passed through air on the outside of tissue. The transmitted dose distributions measured using portal imagers such as SLIC-EPID can be used to verify the dose delivery to a patient. However, several aspects such as accurate calibration procedure and imager response under different conditions should be taken into the consideration. In addition, SLIC-EPID image blurring is another important issue, which should be considered if the SLIC-EPID is used for clinical dosimetry verification.

**Key words:** Head and neck treatment, scanning liquid ionization chamber electronic portal imaging device, segmented intensity modulated radiation therapy, transmitted dose map

## Introduction

The term “transmitted dose” as used in *in vivo* dosimetry, is defined as the dose distribution behind a patient/phantom, can be used for two purposes: verification of dose delivery using

dose distribution behind the patient<sup>[1-6]</sup> and the calculation of dose distribution in the Volume of Interest (VOI) or in the mid-plane of a patient, applying back-projection algorithms to the measured transmitted doses.<sup>[7-12]</sup>


Electronic Portal Imaging Devices (EPIDs) are standard devices incorporated in modern medical linear accelerators. They can be used for a range of tasks in radiation therapy such as patient set-up verification,<sup>[13-18]</sup> dosimetric verification,<sup>[19-27]</sup> and Quality Assurance programs.<sup>[28-37]</sup> Although EPID calibration for two-dimensional dosimetric purposes is a labor-intensive task, after calibration the use of EPID offers significant time efficiency due to the lack of film processing, frequent film calibration and scanning procedure.

Although today, amorphous silicon-based EPIDs (aSi-EPIDs) are the most popular EPIDs incorporated in newly installed linacs, as a result of rapid EPID/linac installation growth in the past decade, many clinical linacs around

### Address for correspondence:

Dr. Mohammad Mohammadi,  
Department of Medical Physics, Royal Adelaide Hospital,  
Adelaide, SA 5000, Australia.  
E-mail: mohammad.mohammadi@health.sa.gov.au

### Access this article online

<b>Quick Response Code:</b> 	<b>Website:</b> <a href="http://www.jmp.org.in">www.jmp.org.in</a>
	<b>DOI:</b> 10.4103/0971-6203.92716

the world still utilize scanning liquid ionization chamber EPIDs (SLIC-EPIDs), especially in developing countries. Furthermore, there are several advantages of SLIC-EPID response. For example, it has been shown that this type of EPIDs is able to detect 0.1 mm Multileaf Collimator (MLC) leaf displacement in Intensity Modulated Radiation Therapy (IMRT) applications<sup>[37]</sup> and it is a suitable device for radiation dose rate evaluation. In contrast, the image blurring for small radiation fields observed in the current study shows there is still need for studies demonstrating the use of SLIC-EPIDs in clinical procedures, e.g. the IMRT.

This study is an EPID dosimetry based assessment of a clinical head and neck IMRT delivery. In a previous study, we have shown that a scanning liquid chamber EPID can be used to verify dose delivery for a segmented intensity modulated radiation therapy (sIMRT) for prostate.<sup>[38]</sup> In order to investigate the SLIC-EPID response in a treatment scenario with more inhomogeneous regions compared to the pelvic area, the current study focuses on a more complex situation in the head and neck. As the first comment, it should be pointed out that throughout the current study, a blurring of electronic portal images (EPIs) was observed for small radiation field sizes. It appears that the blurring can be categorized as two horizontal and vertical linear blurring combined during image acquisition. The impact of additional build-up layer and the conventional jaws positioning on the EPI blurring which occurred for small radiation fields has also been investigated for a range of regular and irregular radiation fields.

## Materials and Methods

A Varian 600CD linear accelerator equipped with a standard 80-leaf MLC and an SLIC-EPID was used. A typical sIMRT MLC sequence file for a head and neck treatment and an anthropomorphic Rando phantom were used. The head and neck sIMRT treatment consisted of five fields applied at gantry angles of 0°, 20°, 230°, 270° and 300°. The minimum and maximum numbers of subfields used in the current study were 10 and 18 for gantry angles of 300° and 230°, respectively. In order to control the undesired beam attenuation effects on the transmitted dose maps, caused by the treatment couch, reported previously as one of the main obstacles in transmitted dose verification,<sup>[38]</sup> the treatment couch was removed from under the head and neck area of the phantom. A sagittal view of the CT dataset including treatment couch, a water equivalent modeled EPID, the Rando phantom and the dose grid matrix used is shown in [Figure 1].

### Extension of CT images for portal dose calculations

The anthropomorphic phantom was scanned using a CT simulator (AcQSim CT, Philips Medical System, Cleveland, OH, USA) with a 3-mm slice thickness and a matrix size of 512 × 512 pixels. In order to model the EPID at 140 cm from the radiation source, the images were then extended

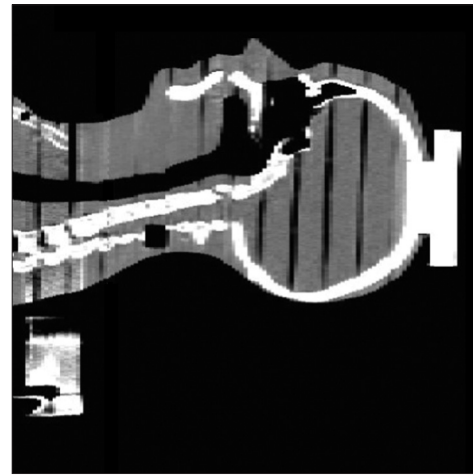


**Figure 1:** A sagittal view of a CT dataset of the Rando phantom and the modeled EPID. The position of treatment couch removed is also shown outside the dose grid region

to 1024 × 1024 pixels by adding rows of pixels with pixel values corresponding to air CT numbers around the acquired CT image.<sup>[38-40]</sup> For non-zero gantry angles, in order to extract the calculated transmitted dose distributions easily through the calculated dose grid matrix, the original CT images were rotated in the opposite direction to the gantry rotation. The routinely available syntax command for image rotation in MATLAB software (MathWorks, Natick, MA, USA) rotates the image around the central point of this image. This command would generally be used to rotate patient CT images for oblique beams. In the current work, due to the non-central position of the tumor site, the extended image was rotated around the center of Region Of Interest (ROI). The results of image rotations around the central point of image were then compared to that rotated around the center of ROI.

### Transmitted dose maps measured using a SLIC-EPID and calculated using Pinnacle<sup>3</sup> Treatment Planning System

#### Transmitted dose maps calculated using Pinnacle<sup>3</sup> TPS

In order to calculate the predicted transmitted dose maps using the available version of Pinnacle<sup>3</sup> Treatment Planning System (TPS; version 6.2b) (ADAC Inc., PHILIPS Medical System, Milpitas, CA, USA), the extended phantom CT data were imported. For both measured and calculated cases, in order to control the extra-transmission through and between MLC leaves, the conventional collimators were placed 1 cm behind the MLCs' position. MLC leaf offset with a value of 0.6 mm was applied manually to the TPS MLC leaf settings for all subfields to account for rounded leaf ends.<sup>[38-40]</sup> As Figure 1 shows, the EPID was then modeled as a 5 × 30 × 30 cm<sup>3</sup> slab behind the phantom. The distance between  $d_{\max}$  of a thin slab of water-equivalent material representing the EPID and the isocenter was set up to be 40 cm [source to EPID distance (SED = 140 cm)]. A corresponding

fraction of 2 Gy total dose was prescribed for each subfield to the isocenter point located inside the anthropomorphic phantom. A three-dimensional dose grid with the voxel size of  $0.175 \times 0.175 \times 0.175 \text{ mm}^3$  was defined to calculate the dose distributions. Due to the limited amount of available computer memory in the TPS computer, the dose grid voxel sizes were defined as  $0.25 \times 0.25 \times 0.25 \text{ mm}^3$  for a gantry angle of  $270^\circ$ . The dose delivered to the phantom and the transmitted dose were calculated using the collapsed cone convolution superposition algorithm. The EPID was modeled with a water-equivalent material. From this model, the dose distribution in the build-up layer was found for all subfields and the transmitted dose extracted.

#### *Transmitted dose maps measured using an SLIC-EPID*

The EPI acquisition and EPID dose calibration procedure are fully explained in literature.<sup>[41-44]</sup> To reduce the effects of fluctuation in EPI pixel values, three consecutive EPIs were acquired for each subfield and averaged. Other procedures were the same as described previously for sIMRT prostate case.<sup>[38]</sup> Details of EPID and treatment planning operating characteristics are shown in [Table 1].

#### *The comparison of the measured and calculated transmitted dose distributions*

The transmitted dose maps measured using an SLIC-EPID and calculated using a Pinnacle<sup>3</sup> TPS were normalized to a point located in a large homogenous area of the irradiated field. In cases where the normalization point is positioned near significant inhomogeneities, especially for small subfields, the uncertainty in the normalization factor is greater. Using an in-house code written in MATLAB and due to the SLIC-EPID pixel size ( $1.27 \text{ mm} \times 1.27 \text{ mm}$ ), both sets of transmitted dose maps were then compared using the gamma function algorithm for each subfield and

the corresponding accumulated fields with the  $\Delta D_{\text{max}}$  and Distance To Agreement (DTA) criteria of  $3\%/2.54 \text{ mm}$ .<sup>[45]</sup>

After evaluating individual subfields, the corresponding total field transmitted dose maps were then created by multiplying the relative weighting factor contribution with the dose for each subfield. The corresponding calculated transmitted dose maps for the total fields were also prepared by adding up all of the subfields. The measured and calculated total transmitted dose maps were normalized to a point located in an approximately homogeneous area located inside the MLC field.

#### **SLIC-EPID response for small radiation fields**

Since blurring was observed in some small radiation fields during SLIC-EPI acquisition, several issues including the smallest field size with sharp edges, the impact of additional build-up layer on the EPI quality and the impact of conventional jaws were evaluated.

#### *The impact of additional build-up layer*

Several EPIs were acquired for nominal square radiation field sizes from  $1 \times 1$  to  $5 \times 5 \text{ cm}^2$ , using conventional jaws with and without an additional build-up layer (5mm RW3 layer<sup>[41]</sup>).

To prevent the impact of statistical fluctuations on EPIs, for each set-up, three consecutive EPIs were acquired, averaged and converted to the radiation fluence map, which is the radiation beam reaching the EPID in the absence of patient phantom or any other attenuator<sup>[42]</sup>. Two series of acquired EPIs (with/without an additional build-up layer) were acquired and the raw SLIC-EPIs were then converted to the radiation fluence map. The results were then compared with those measured using Extended Dose Range 2 (EDR2) film under the same conditions.

#### *The impact of conventional jaws positioning*

The impact of conventional jaws positioning on the blurring of EPIs acquired for small MLC fields was also explored. Setting up the conventional jaws in various positions, the impact of intra/inter leaf leakage on the EPI blurring was investigated. This was performed for two groups of MLC fields: firstly, small fields and secondly, the small fields in the presence of larger fields. The conventional jaws were positioned far from MLC leaf positioning ( $14 \times 20 \text{ cm}^2$ ) and also close to the opened MLC leaf positions ( $0.5 \text{ cm}$  behind). The corresponding absolute dose difference was then evaluated.

#### **SLIC-EPID response for high dose gradient regions**

In order to investigate the TPS and the SLIC-EPID response at the interface between air and phantom, the homogenous phantom (10 cm thick water-equivalent material), used to verify the proposed calibration procedure, was shifted by 2 cm in the direction of the  $x$  and  $y$  axes.

**Table 1: SLIC-EPID and Pinnacle<sup>3</sup> TPS set-ups for portal dosimetry**

<i>SLIC-EPID</i>	
Beam energy	6 MV
Dose rate	300 MU/min
Source to EPID distance	140 cm
Extra build-up layer	5 mm
Matrix type	Full resolution
Frame average	1
Read-out mode	Fast
Treatment Planning System	
Dose calculation algorithm	CC super-position
Dose grid voxel size	$0.25 \times 0.25 \times 0.25 \text{ mm}^3$
Modeled EPID	$5 \times 30 \times 30 \text{ cm}^3$ water-equivalent material
Conventional collimators' position	1 cm behind MLCs
MLC leaf offset	0.6 mm
Dose calculation algorithm	CC super-position
SLIC-EPID: Scanning liquid ionization chamber electronic portal imaging device	

Using a  $17 \times 17 \text{ cm}^2$  radiation field size, the homogenous phantom was positioned so that a part of the radiation beam passed through the air. The measured and calculated transmitted dose maps were then compared using relative dose difference map and gamma function algorithm, with 3%/2.54 mm criteria.

## Results and Discussion

### Extension of CT images for portal dose calculations

The position of the central point of a CT image and the center of an ROI is shown in [Figure 2a]. In addition, the difference in the CT numbers between a CT image rotated to  $60^\circ$  around the central point of the CT image (green point) and around the Point of Interest (POI) (red point) is illustrated in [Figure 2b]. The area affected by possible fluctuation of CT number, due to the use of image processing for image rotation (approximately  $\pm 50$ ),<sup>[38]</sup> is shown in gray scale. The variation of CT numbers affects the dose delivery plans calculated using a treatment planning system. A significant variation in CT numbers was observed in the high CT number gradient

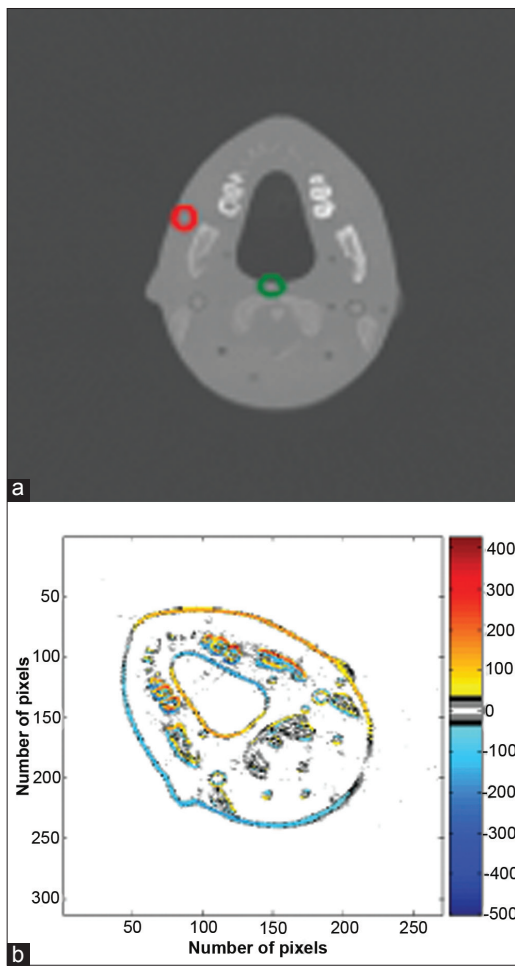


Figure 2: (a) Raw CT image for head and neck region of the Rando phantom at AP direction;(b) the CT number difference for a CT image rotated around the central point of the image and around the central point of the ROI

regions. A maximum difference of  $\pm 500$  in CT numbers was observed in the edge of inhomogeneities. Cross-plane and inplane profiles of the image rotated around the central point of image and around the central point of POI are shown in [Figure 3]. The corresponding CT number difference is also shown as a secondary axis. These line profiles show that in the boundaries of inhomogeneities, a significant variation of CT numbers was observed.

In the transmitted dose calculation for the prostate case,<sup>[38]</sup> because of the ROI positioning in the central part of a patient (consequently in the central region of the images), the conventional image rotation does not affect the results significantly. Additionally, the prostate and surrounding regions are more homogenous than the head and neck sites. In contrast, for ROIs located outside the central region of the body, the rotation around the image center will cause artifacts. Therefore, the patient CT images must be rotated around the central point of the target volume.

### Transmitted dose maps measured using an SLIC-EPID and calculated using Pinnacle<sup>3</sup> TPS

The corresponding relative dose difference and gamma maps for a typical series of relative transmitted dose maps are shown in [Figure 4]. It refers to several radiation subfield obtained from an oblique beam (gantry angle of  $230^\circ$ ). The x and y axes of all images represent the number image pixel number. The relative dose differences and the corresponding gamma maps show that a good agreement was observed inside the radiation fields for most MLC subfields. Several disagreeing regions were observed in the

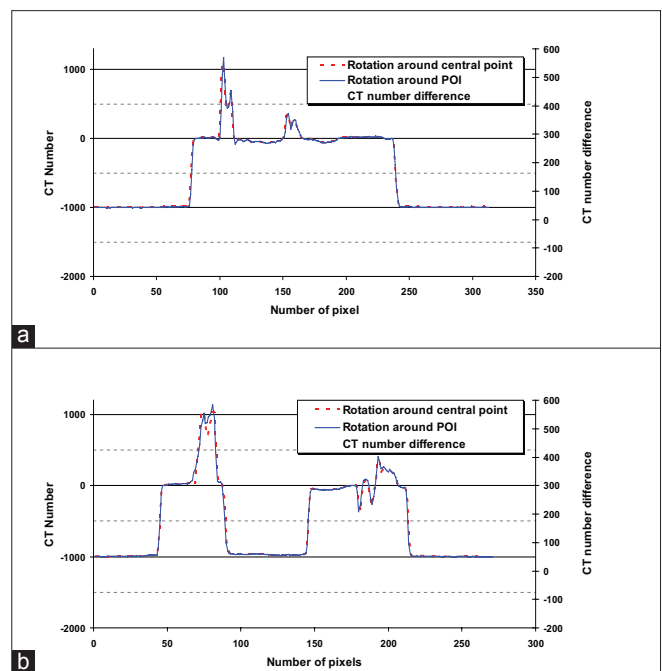


Figure 3: (a) Inplane and (b) cross-plane profiles of two CT images rotated to  $60^\circ$  gantry angle around the central point of the image, around the POI and the corresponding CT number difference



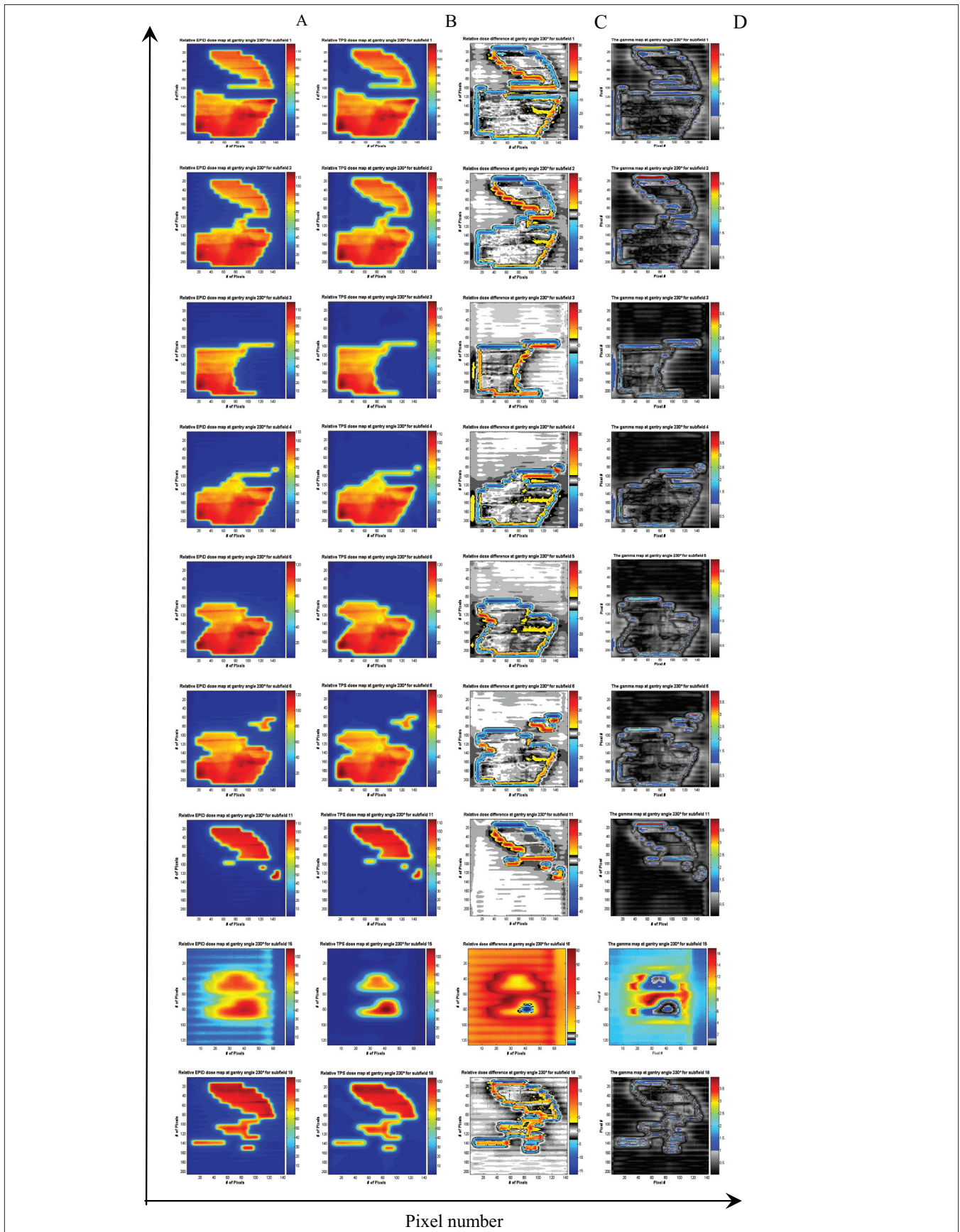


Figure 4: Transmitted dose maps measured and calculated using SLIC-EPID and Pinnacle<sup>3</sup> TPS, the corresponding relative dose difference and gamma maps for subfields acquired for the gantry angle of 230°. The gamma function criteria are 3%/2.54 mm for all cases

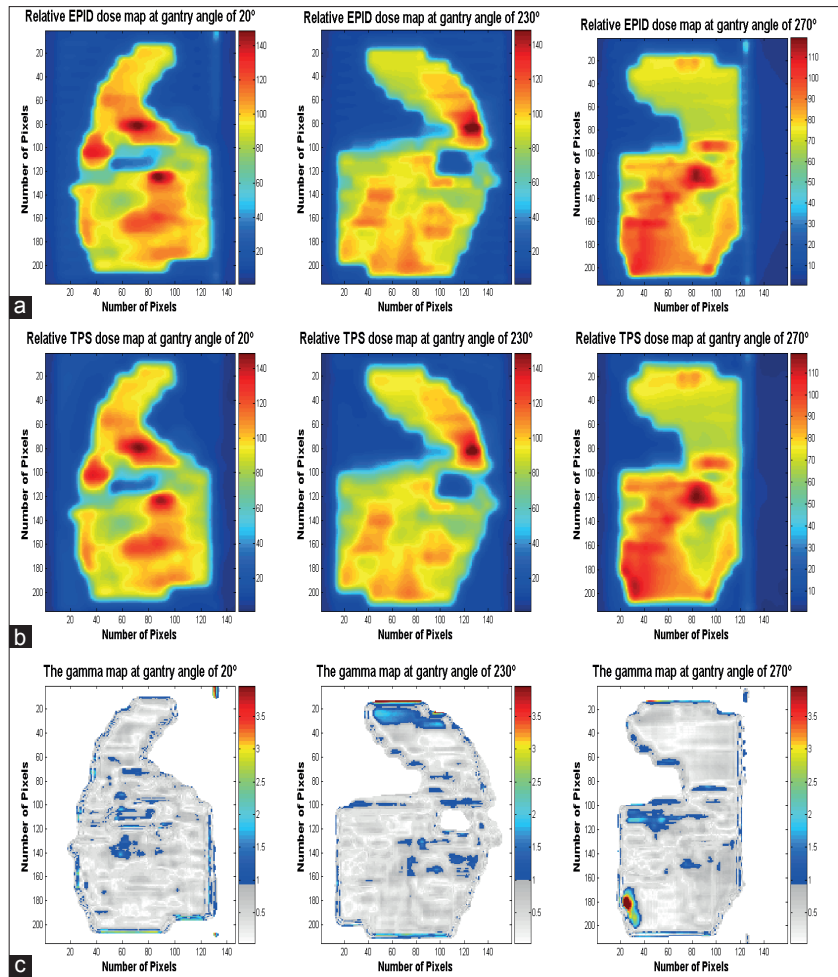


Figure 5: (A series) Total field transmitted dose maps, (B series) calculated transmitted dose maps, (C series) relative dose differences, and (D series) the corresponding gamma maps with criteria of 3%/2.54 mm at gantry angles of 0°, 20°, 230°, 270°, and 300°

Table 2: The agreement percentages between relative transmitted and the corresponding calculated dose maps (the gamma criteria were 3%/2.54 mm)

Subfield	Agreement percentage between subfields and total field of simRT fields (%)				
	Field 1 (0°)	Field 2 (20°)	Field 3 (230°)	Field 4 (270°)	Field 5 (300°)
1	95.7	95.7	91.0	94.3	92.6
2	95.1	92.9	91.7	95.00	93.6
3	94.2	94.7	93.3	95.2	91.7
4	94.5	95.0	94.4	96.2	91.3
5	94.1	93.6	96.7	96.0	84.3
6	95.4	94.0	94.4	96.6	46.8
7	97.6	93.9	94.5	97.3	22.6
8	87.0	50.4	92.7	97.4	29.4
9	88.3	2.1	95.9	36.9	72.1
10	89.0	93.4	96.5	5.2	89.4
11	2.6	92.7	96.3	96.4	-
12	2.2	93.5	0.7	-	-
13	21.8	95.1	94.2	-	-
14	52.8	95.5	2.3	-	-
15	90.5	95.7	6.2	-	-
16	92.5	-	98.3	-	-
17	-	-	97.7	-	-
18	-	-	95.9	-	-
Total field	86.7	90.2	89.8	88.6	82.3

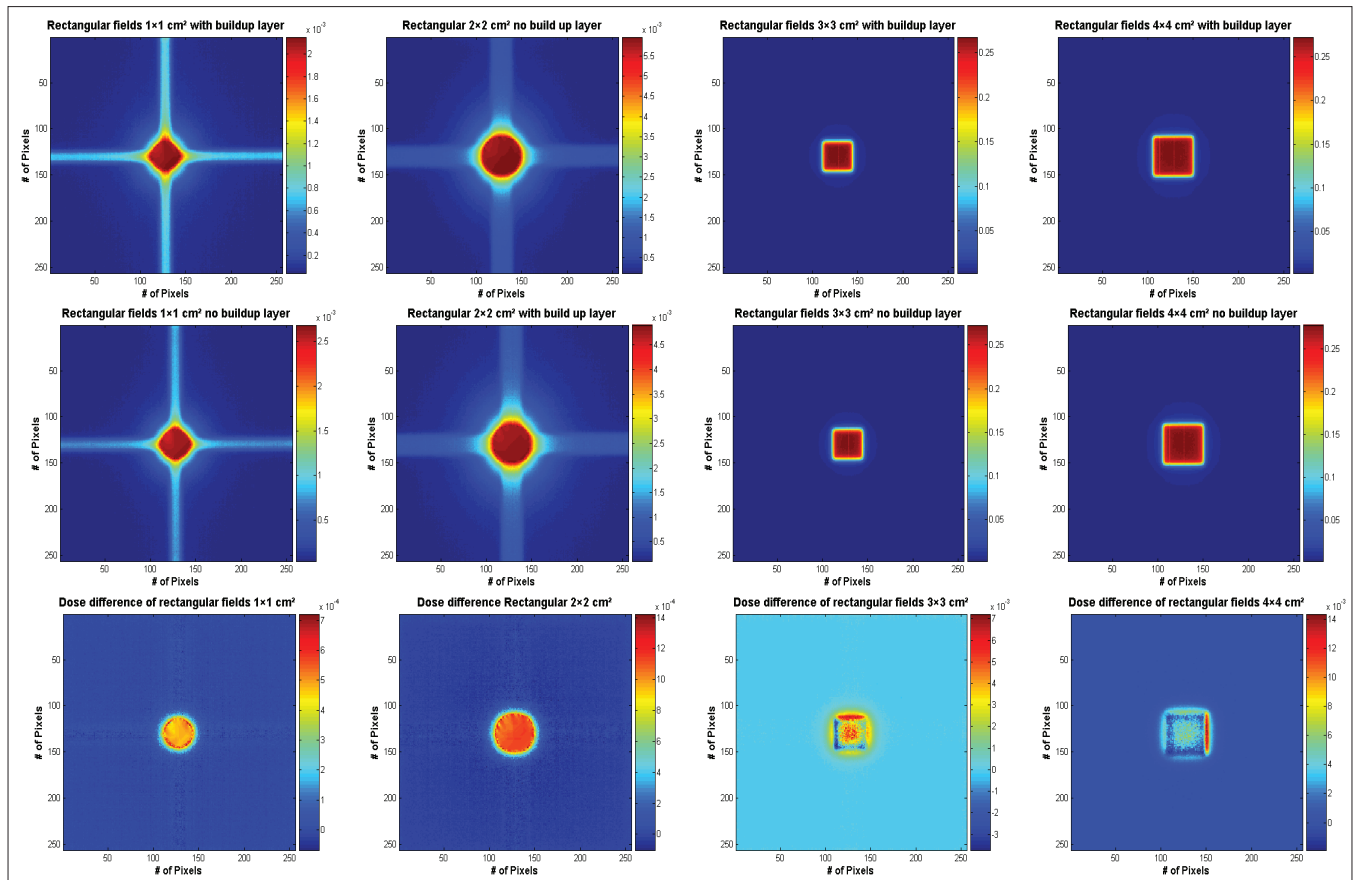


Figure 6: The primary fluence maps with build-up layer (first row), without build-up layer (second row), and corresponding dose difference maps (third row) for small radiation field sizes for 1 × 1, 2 × 2, 3 × 3 and 4 × 4 cm<sup>2</sup>

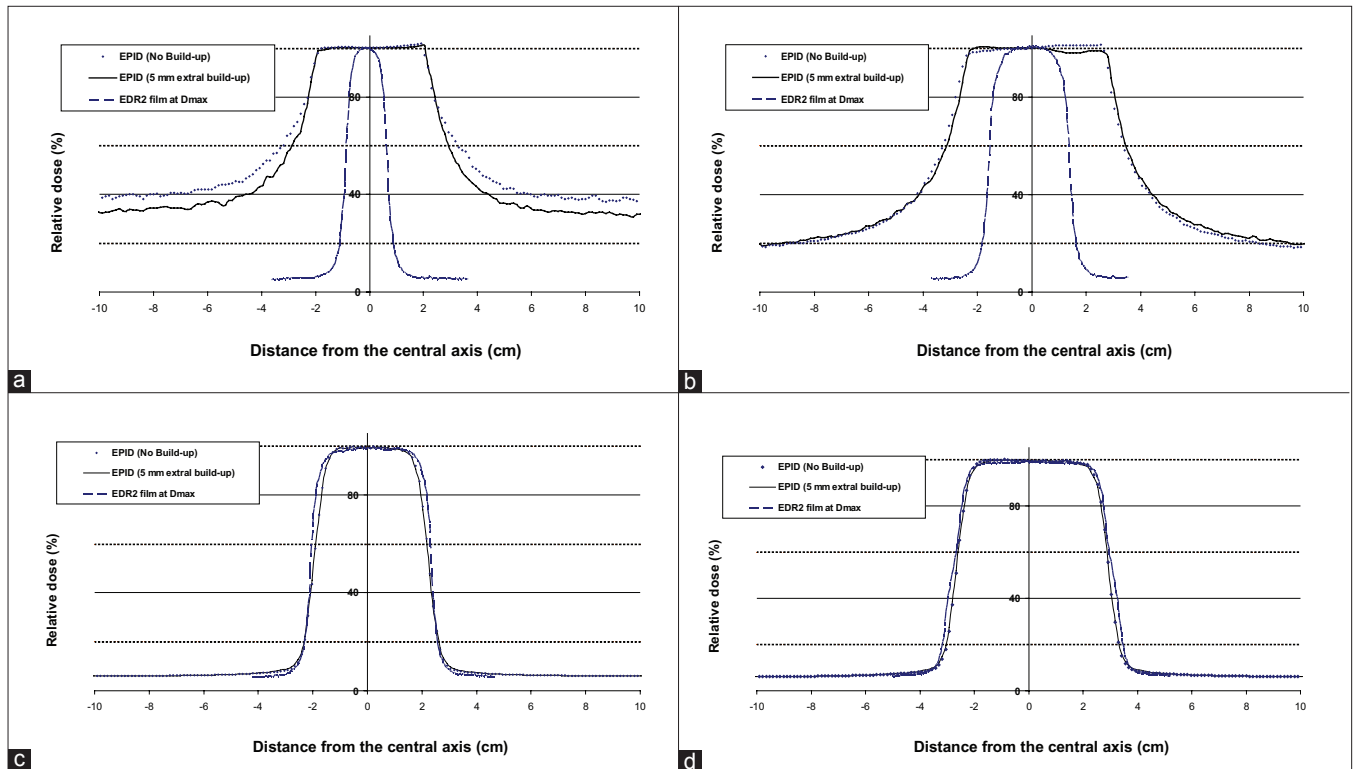


Figure 7: The cross-plane profiles measured for several small fields (a) 1 × 1 cm<sup>2</sup>, (b) 2 × 2 cm<sup>2</sup>, (c) 3 × 3 cm<sup>2</sup> and (d) 4 × 4 cm<sup>2</sup>, achieved from transmitted dose maps measured using SLIC-EPID and EDR2 films at a distance of 140 cm

penumbral areas and more significant discrepancies were also observed for several small subfields (2 of 18 subfields) used routinely to boost the dose delivered to the central part of the tumor site. The size of subfields with significant inconsistencies was found to be less than 8 cm<sup>2</sup>.

The total field relative to measured and calculated transmitted dose maps, the relative dose difference and the corresponding gamma maps are shown in [Figure 5] for all five gantry positions used in the current work. Although

inaccuracy in the positioning of the normalization points and the possible misalignment of the corresponding subfields decreases the correlation between measured and calculated dose distributions, an acceptable consistency was observed inside the ROIs for all gantry positions.

In order to provide more information on the agreement between measured and calculated transmitted dose distributions for each subfield and for the corresponding total field, the gamma scores for all evaluated subfields and

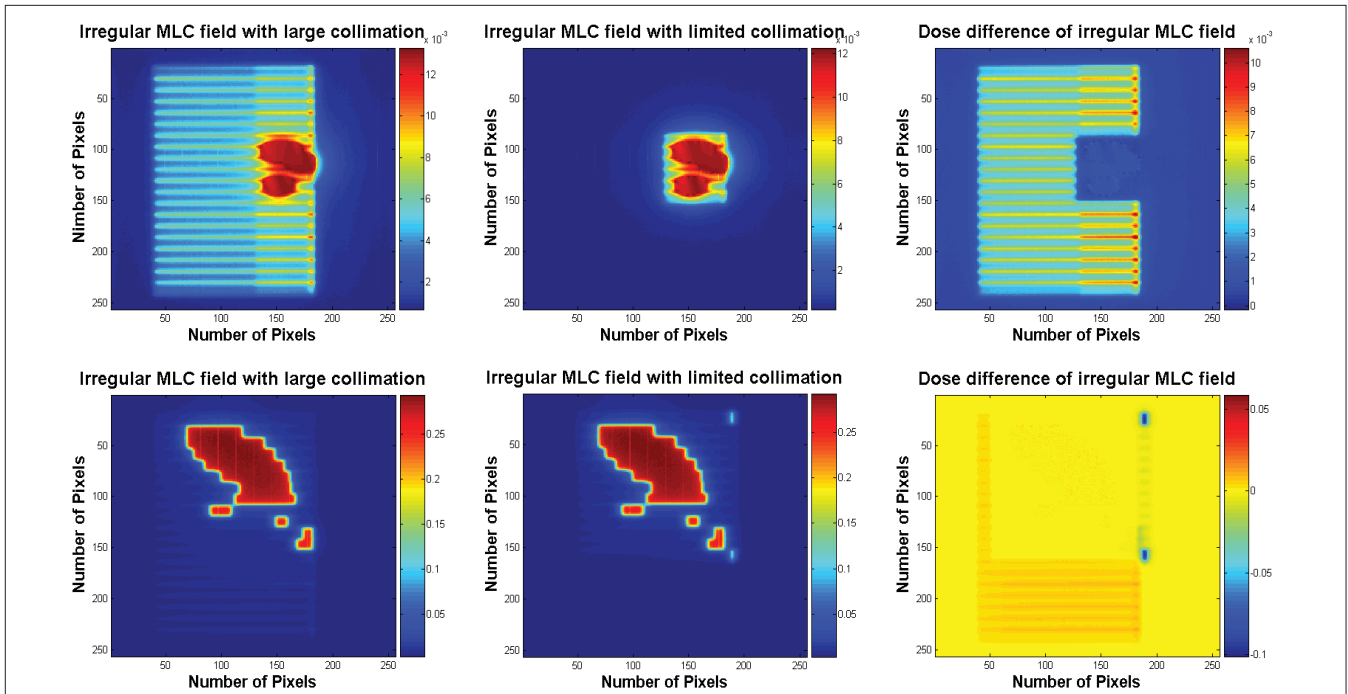


Figure 8: Absolute transmitted dose maps of MLC fields with the jaws positioned away and close to the MLC field and the corresponding absolute dose difference map for small MLC fields; several small fields in the vicinity of a large irradiated area

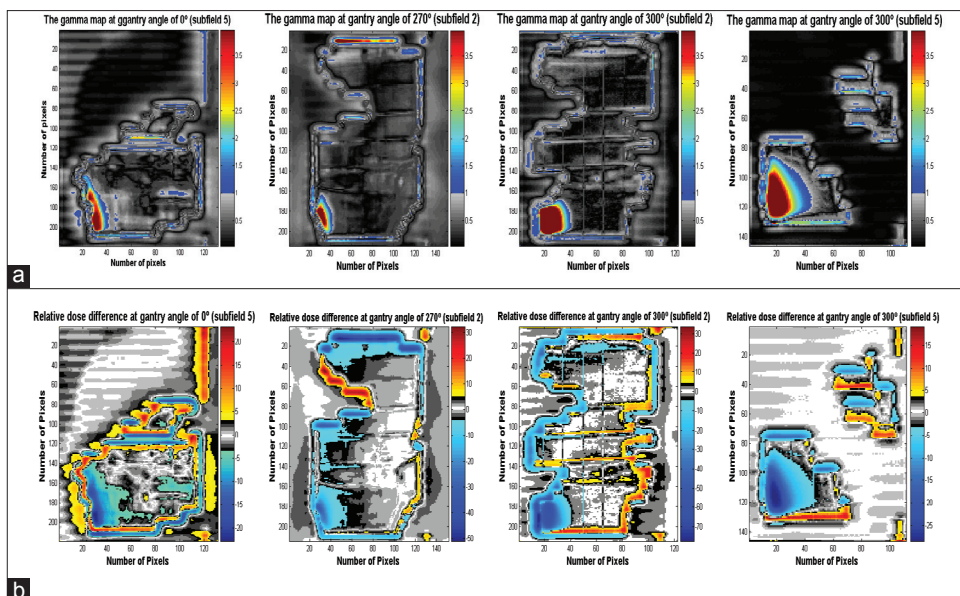


Figure 9: (a) The gamma and (b) the dose difference maps for typical radiation subfields at AP direction, 270° and 300°. The PASSED area for gamma criteria and dose difference within 3% for dose difference maps are shown in gray



total fields are given in [Table 2]. Due to the blurring of the EPIs, for subfields smaller than  $8 \text{ cm}^2$  (these are used to boost the radiation in the active tumor regions), several significant inconsistencies were observed.

The average agreement for these subfields was found to be less than 39.5%. The result for a typical small MLC field is shown in Figure 4 (see subfield 15). The relative dose difference values for regions outside the MLC fields were found to be greater than 3% of the dose delivered to the central part of MLC field, defined as the dose difference criterion for gamma assessment. Discarding the results for small fields, the maximum, minimum and average gamma score for all subfields were found to be 98.3%, 72.1% and 92.6%, respectively.

As a result (the agreement between two series of consecutive EPIs is approximately 99%), so it can be said that for most fields, there is an excellent agreement between TPS and EPID transmitted dose distributions.

In some subfields and consequently in the accumulated total fields, several significant differences were observed between measured and calculated transmitted dose maps inside the MLC fields and outside the patient anatomy. The relative dose differences in these regions were found to be greater than 6% for all subfields observed for two series of data sets acquired at A-P direction and at the gantry angle of  $300^\circ$ . The calculated dose values were found to be greater than those measured using SLIC-EPID in all these cases.

The reasons for the differences between the calculated and measured transmitted dose maps were investigated.

The first group of inconsistencies was for small fields (smaller than  $8 \text{ cm}^2$  at the isocenter). EPI blurring was found to be the main source of uncertainty. The second group of inconsistencies referred to several subfields for which not all parts of the radiation beam were incident on the phantom, but were passing through air. Although this type of discrepancy is irrelevant to the transmitted dose passing through the patient, the gamma score, for the MLC fields affected by this problem, decreases significantly. These two important issues are discussed in the following sections.

### Evaluation of EPI blurring for small radiation fields The impact of additional build-up layer

Typical radiation fluence maps for field sizes from  $1 \times 1 \text{ cm}^2$  to  $4 \times 4 \text{ cm}^2$  are shown in Figure 6 for an SED of 140 cm at  $D_{\text{max}}$ . The x and y axes represent the number of pixels for all cases. A significant blurring of EPIs was observed for  $1 \times 1$  and  $2 \times 2 \text{ cm}^2$  radiation field sizes acquired both with and without the build-up layer. The absolute dose difference map between two averaged EPIs shows that the additional build-up layer increases uniformly the EPI pixel values in the blurred area, as is expected. Two horizontal and vertical strip bands, exactly the width of the radiation field size, were observed for radiation field sizes smaller than  $9 \text{ cm}^2$ . The width of strip bands was found to be the same size as the radiation field size. This shows that the scanning of the row and column processing in the SLIC-EPID affects the pixel values. In addition, two effects are also discussed by Van Herk *et al.* for different image resolution in horizontal and vertical directions as follows: The 256-electrometer amplifiers including an appropriate filter mostly are known to be responsible for vertical blurring, and the lack of shielding between liquid ionization chambers is reported to

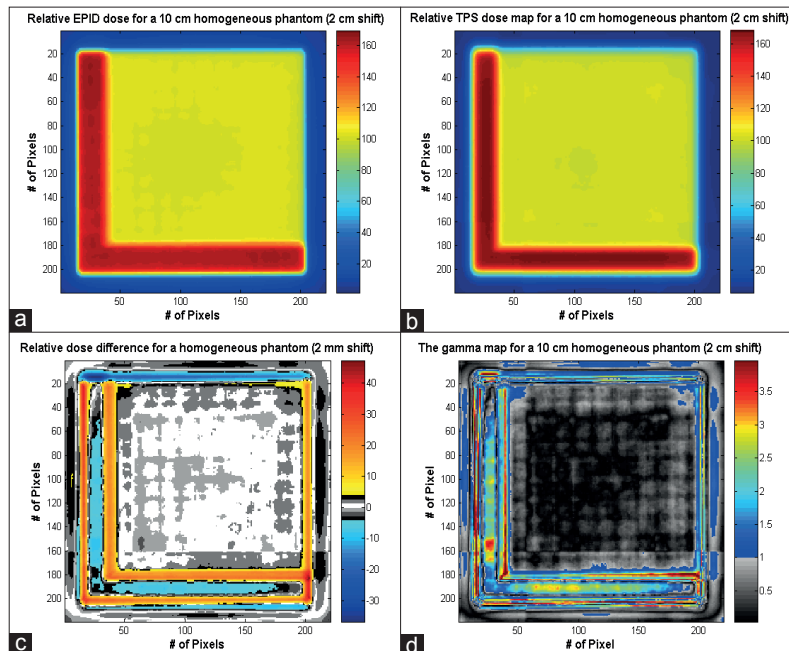
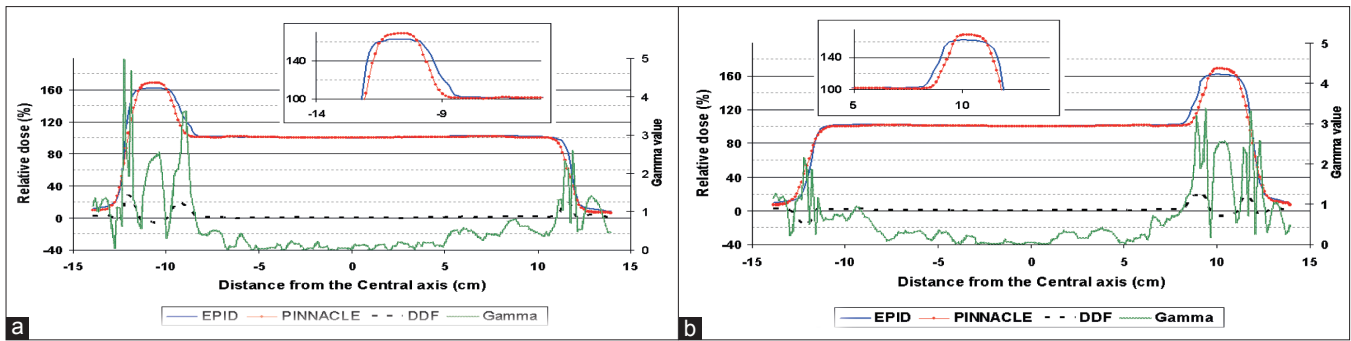


Figure 10: (a and b) Relative measured and calculated dose for a  $17 \times 17 \text{ cm}^2$  field size for a 2-cm shifted 10-cm homogeneous attenuator in x and y axes directions; (c and d) the corresponding relative dose difference and gamma maps with criteria of 3%/2.54 mm



**Figure 11: (a) Cross-plane and (b) inplane profiles of the measured and calculated relative dose maps, the corresponding relative dose difference and gamma map with 3%/2.54 mm criteria for a  $17 \times 17\text{cm}^2$  field size for a 2-cm shifted 10-cm homogenous attenuator**

be potentially responsible for spurious sensitivity outside the pixel area in the direction which is aligned with the electric field lines. Figures 7 and 8 show that the blurring in the electric field direction (horizontal direction) is quite larger than in the vertical direction. It has also been shown the detective quantum efficiency (DQE) increases for ionization detectors with the decrease of the dose. If the radiation dose, delivered to SLIC-EPID ionization chambers, is originally averaged for each row or column reading, this justifies the probability of blurring that happened in SLIC-EPID during small field radiation dose deliveries.<sup>[46, 47]</sup>

The corresponding cross-plane profiles for small fields (from  $1 \times 1\text{ cm}^2$  to  $4 \times 4\text{ cm}^2$ ), measured using SLIC-EPID with and without extra build-up layer and using EDR Kodak Film (EDR2), are also shown in [Figure 7]. EDR2 films have been reported to have a linear dose–response region extending to 500 cGy.<sup>[48]</sup> Results show that for  $1 \times 1\text{ cm}^2$  and  $2 \times 2\text{ cm}^2$  fields, SLIC-EPIDs are not able to create a reliable dose map. In contrast, with the increase of radiation field size, the data collected by SLIC-EPID match well with those collected using EDR2 films. The uncertainties at strip lines depend on the field size and increase with the increase of radiation field size.

Due to the consistency between dose maps and the corresponding dose difference maps shown in Figure 6, as well as results shown in Figure 7, it was concluded that the additional build-up layer has no significant effect on the blurring of small field images. The additional build-up layer increases the number of free electrons reaching the EPID sensitive layer and the contribution of scattered photons.<sup>[49]</sup> More scattering increases the “fog phenomenon” in EPIDs, and this decreases the sharpness of EPI. The horizontal and vertical strip bands show that the scanning of the row and column processing in the SLIC-EPID affects the pixel values. Random image blurring was observed in some of the small fields. However, since small fields are only used for boost dose delivery and their field size contribution is a small fraction (1% to 3%) of the total field size, this small field blurring had a negligible effect on overall image quality for the independent gantry angles used in this

study. This is the main reason (or quantitative reason to say the inconsistencies are irrelevant for dose verification); however, this is reported as a drawback of SLIC-EPID.

### *The impact of conventional jaws positioning*

Typical results of conventional jaws positioning affecting the amount of MLC leakage on the blurring of EPIDs acquired for small MLC fields are shown in [Figure 8]. In the first row of the figure, a small MLC field with three separated areas is shown. The conventional jaws were positioned far behind MLC leaf positioning ( $14 \times 20\text{ cm}^2$ ) (first column) and also close to the opened MLC leaf positions (0.5 cm behind) (second column). The corresponding absolute dose difference is also displayed. As the image acquisition time is limited, no saturation is observed. Due to the blurring observed in the EPIDs, three small fields cannot be distinguished. The absolute dose difference map shows that the impact of jaw positioning, and therefore intra- and inter-leaf MLC leaf leakage, does not either remove or reduce the blurring effect.

Although the blurring effect is observed in EPIDs acquired using SLIC-EPID for small radiation fields, in the presence of large irradiated areas, the small irradiated areas can be detected clearly. As the second row in Figure 8 shows, no blurring was observed for small MLC fields (less than  $9\text{ cm}^2$ ) when there is a large irradiated area in the vicinity of small fields. In this case, no significant difference was observed for retracted and closed jaw positioning.

SLIC-EPIDs, like other EPIDs, are generally developed to acquire an EPI for large open fields to verify patient positioning. It can be assumed, therefore, that the row and column scanning procedure as well as the supporting software do not process correctly the EPIDs acquired for small radiation fields. No significant effect of the additional build-up layer and conventional jaws positioning was found on the blurred EPIDs. The main reason for this is not exactly clear. The vertical and horizontal strips show that the supporting SLIC-EPID image construction including hardware and software could be responsible for EPI blurring because there is no radiation deposition in

the off-axis areas.

### *SLIC-EPID response for high dose gradient regions*

Several discrepancies between EPID measurements and TPS calculations were observed in the peripheral part of the MLC radiation fields. Typical gamma maps obtained from EPID and TPS comparisons for subfields of field 1 (AP direction), field 4 (gantry angle 270°) and field 5 (gantry angle of 300°) are shown in [Figure 9]. All of the significant disagreements were found to be located in the areas where beams were passing through air (outside the RANDO phantom). As all gamma maps show (series a), there is a good agreement for gamma maps in regions where the radiation beam passed through the patient/phantom. In contrast, significant discrepancies exist for radiation field sites where the beam is passing through the air. The corresponding relative dose difference maps (series b) show that the TPS relative dose values are greater than those measured using SLIC-EPID for disagreeing areas.

In order to find the reason for this discrepancy in the particular part of the gamma maps, two possibilities were investigated. Firstly, there was a concern about the calibration method used in this work, particularly for the off-axis correction performed using EDR2 films.<sup>[42, 44]</sup> The second concern was about how the EPID or the TPS responded at the interface between inhomogeneities. It has been shown that in the presence of homogenous attenuators, there is a reasonable agreement between EPID and TPS dose values for large radiation fields.<sup>[43, 44]</sup> The results prove that the calibration method used in this study guarantees sufficient accuracy when using the EPID dosimetry.

The measured and calculated transmitted dose maps, corresponding relative dose difference, and gamma maps are indicated in [Figure 10] and the corresponding line profiles are shown in [Figure 11]. The results showed that after normalization to the central point located in the homogeneous phantom region, a significant discrepancy was observed between the measured and calculated transmitted dose maps in the area corresponding to the air region. In addition, the relative dose difference map showed that at all points where the beam portion passes through the air, the dose calculated using TPS is always greater than that measured using SLIC-EPID. Moreover, the area irradiated through the air for EPID measurements was found to be wider than those calculated using TPS.

Discrepancies between TPS and EPID dose profiles in the air areas can arise due to EPI construction. Two factors, SLIC-EPID hardware and data processing software, allow the EPID output to change. By using a 1mm liquid film (Isooctane, spectroscopical pure, Merck) as an ionization medium,<sup>[50]</sup> the SLIC-EPID ionization chambers are not quite independent and each pixel value can be affected by the neighboring pixels located in the surrounding region.

The impact of software used to construct the EPI should also be taken into consideration.

Several modifications including offset, dark field and flood field corrections, that are defined in the image acquisition software (PortalVision LC250, Varian Medical System Inc, Baden Switzerland), have been used to construct EPI. Moreover, several additional corrections such as filtering, linear correction and linear fix correction algorithms can be applied following the image acquisition.<sup>[51]</sup> These corrections control the undesired noise and help to smooth EPI pixel values. Through these procedures, it is expected that the EPID response would be lower values and larger areas than that calculated using TPS for the same conditions.

The output of the TPS on the interface between air and phantom should also be taken into account. The TPS, Pinnacle<sup>3</sup> (version 6.2) calculates the dose with the collapsed cone convolution superposition algorithm.<sup>[52, 53]</sup> This algorithm is based on average density scaling method rather than a local density scaling. The scaling leads to the overdose/underdose calculation results compared to the measurements and Monte Carlo simulations.<sup>[54]</sup>

## **Conclusion**

Several issues including EPI blurring and differences observed between calculated and measured transmitted dose maps, due to inaccurate beam modelling using treatment planning system and routine measurements uncertainties, decrease the accuracy of transmitted dose measurements. However, due to the small size of these radiation fields and their contribution, the impact of blurred EPIs on the total field evaluation is negligible. Moreover, the significant inconsistencies occurring between measured and calculated dose maps were shown to be located in regions of air transmission and are thus irrelevant to patient dose delivery verification.

The dose delivery verification for a head and neck sIMRT case using SLIC-EPID was investigated. For large MLC fields, an excellent agreement was observed between transmitted dose measured using SLIC-EPID and that calculated by TPS (gamma score approximately 95%). For several small subfields, however, due to EPI blurring, a significant disagreement was found in the gamma results. Additionally, a significant disagreement between EPID and TPS dose maps was found in several parts of the radiation subfields, when the radiation beam passed through air.

The transmitted dose distributions measured using portal imagers such as SLIC-EPID can be used to verify the dose delivery to the patient. However, several issues such as accurate calibration procedure and imager response under different conditions should be taken into consideration. For instance, the procedure of image construction using an

SLIC-EPID reduces the quality of EPIs acquired for small fields. In addition, SLIC-EPID response differs from TPS response when a large inhomogeneity, e.g. a large air pocket, is positioned in the radiation beam path.

## Acknowledgment

The work was supported by Royal Adelaide Hospital and the School of Physics and Chemistry of the University of Adelaide. Authors also would like to thank Dr Paul Reich for his support and assistance with this project.

## References

- Chang J, Mageras GS, Chui CS, Ling CC, Lutz W. Relative profile and dose verification of intensity-modulated radiation therapy. *Int J Radiat Oncol Biol Phys* 2000;47:231-240.
- Kirby MC, Williams PC. Measurement possibilities using an electronic portal imaging device. *Radiother Oncol*. 1993;29:237-243.
- Reich P, Bezak E, Mohammadi M, Fog L. The prediction of transmitted dose distributions using a 3D treatment planning system. *Australas Phys Eng Sci Med* 2006;29:18-29.
- Boellaard R, van Herk M, Uiterwaal H, Mijnheer B. First clinical tests using a liquid-filled electronic portal imaging device and a convolution model for the verification of the midplane dose. *Radiother Oncol* 1998;47:303-12.
- Lin MH, Chao TC, Lee CC, Tung CJ, Yeh CY, Hong JH. Measurement-based Monte Carlo dose calculation system for IMRT pretreatment and on-line transit dose verifications. *Med Phys* 2009;36:1167-75.
- van Zijtveld M, Dirkx M, Breuers M, de Boer H, Heijmen B. Portal dose image prediction for *in vivo* treatment verification completely based on EPID measurements. *Med Phys* 2009;36:946-52.
- Boellaard R, van Herk M, Mijnheer BJ. A convolution model to convert transmission dose images to exit dose distributions. *Med Phys*. 1997;24:189-99.
- Hansen VN, Evans PM, Swindell W. The application of transit dosimetry to precision radiotherapy. *Med Phys*. 1996;23:713-21.
- Huyskens D, Van Dam J, Dutreix A. Midplane dose determination using *in vivo* dose measurements in combination with portal imaging. *Phys. Med. Biol* 1994;39:1089-1101.
- van Elmpt WJ, Nijsten SM, Mijnheer BJ, Minken AW. Experimental verification of a portal dose prediction model. *Med Phys* 2005; 32:2805-18.
- Ansbacher W. Three-dimensional portal image-based dose reconstruction in a virtual phantom for rapid evaluation of IMRT plans. *Med Phys* 2006;33:3369-82.
- Wendling M, McDermott LN, Mans A, Sonke JJ, van Herk M, Mijnheer BJ. A simple backprojection algorithm for 3D *in vivo* EPID dosimetry of IMRT treatments. *Med Phys* 2009;36:3310-21.
- Kaatee RS, Olofsen MJ, Verstraate MB, Quint S, Heijmen BJ. Detection of organ movement in cervix cancer patients using a fluoroscopic electronic portal imaging device and radiopaque markers. *Int J Radiat Oncol Biol Phys* 2002;54:576-83.
- Bel A, Vos P, Rodrigus P, Creutzberg C, Visser A, Stroom J, *et al*. High-precision prostate cancer irradiation by clinical application of an offline patient setup verification procedure, using portal imaging. *Int J Radiat Oncol Biol Phys*. 1996;35:321-32.
- Brock K, McShan D, Balter J. A comparison of computer-controlled versus manual on-line patient setup adjustment. *J Appl Clin Med Phys* 2002;3:241-7.
- Briere TM, Beddar S, Balter P, Murthy R, Gupta S, Nelson C, *et al*. Respiratory gating with EPID-based verification: the MDACC experience. *Phys Med Biol* 2009;54:3379-91.
- Lawson JD, Wang JZ, Nath SK, Rice R, Pawlicki T, Mundt AJ, *et al*. Intracranial application of IMRT based radiosurgery to treat multiple or large irregular lesions and verification of infra-red frameless localization system. *J Neurooncol* 2009.
- Penninkhof J, Quint S, Boer H, Mens JW, Heijmen B, Dirkx M. Surgical clips for position verification and correction of non-rigid breast tissue in simultaneously integrated boost (SIB) treatments. *Radiother Oncol* 2009;90:110-5.
- Bogaerts R, Van Esch A, Reyman R, Huyskens D. A method to estimate the transit dose on the beam axis for verification of dose delivery with portal images. *Radiother Oncol*. 2000;54:39-46.
- Symonds-Taylor JRN, Partridge M, Evans PM. An electronic portal imaging device for transit dosimetry. *Phys. Med. Biol* 1997; 42:2273-83.
- Essers M, Hoogervorst BR, van Herk M, Lanson H, Mijnheer BJ. Dosimetric characteristics of a liquid-filled electronic portal imaging device. *Int. J. Radiat. Oncol. Biol. Phys.* 1995;33:1265-72.
- Parsaei H, el-Khatib E, Rajapakse R. The use of an electronic portal imaging system to measure portal dose and portal dose profiles. *Med Phys*. 1998;25:1903-9.
- Kroonwijk M, Pasma KL, Quint S, Koper PC, Visser AG, Heijmen BJ. *In vivo* dosimetry for prostate cancer patients using an electronic portal imaging device; demonstration of internal organ motion. *Radiother Oncol*. 1998;49:125-32.
- Van Esch A, Depuydt T, Huyskens DP. The use of an aSi-based EPID for routine absolute dosimetric pre-treatment verification of dynamic IMRT fields. *Radiother Oncol*. 2004;71:223-34.
- de Boer J, Heijmen B, Pasma K, Visser A. Characterization of a high-elbow, fluoroscopic electronic portal imaging device for portal dosimetry. *Phys Med Biol* 2000;45:197-216.
- van Elmpt WJ, Nijsten SM, Schiffeleers RF, Dekker AL, Mijnheer BJ, Lambin P, *et al*. A Monte Carlo based three-dimensional dose reconstruction method derived from portal dose images. *Med Phys* 2006;33:2426-34.
- Richter A, Sweeney R, Baier K, Flentje M, Guckenberger M. Effect of breathing motion in radiotherapy of breast cancer: 4D dose calculation and motion tracking via EPID. *Strahlenther Onkol* 2009;185:425-30.
- Kirby MC, Williams PC. The use of an electronic portal imaging device for exit dosimetry and quality control measurements. *Int J Radiat Oncol Biol Phys* 1995;31:593-603.
- Liu G, van Doorn T, Bezak E. Assessment of flatness and symmetry of megavoltage X-ray beam with an electronic portal imaging device. *Australas Phys Eng Sci Med* 2002;25:58-66.
- Menon GV, Sloboda RS. Compensator quality control with an amorphous silicon EPID. *Med Phys*. 2003;30:1816-24.
- Pasma K, Kroonwijk M, van Dieren E, Visser A, Heijmen B. Verification of compensator thicknesses using a fluoroscopic electronic portal imaging device. *Med Phys*. 1999;26:1524-9.
- Menon GV, Sloboda RS. Quality assurance measurements of a-Si EPID performance. *Med Dosim*. 2004;29:11-17.
- Chang J, Obcemea CH, Sillanpaa J, Mechalakos J, Burman C. Use of EPID for leaf position accuracy QA of dynamic multi-leaf collimator treatment. *Med Phys* 2004;31:2091-6.
- Beck JA, Budgell GJ, Roberts DA, Evans PM. Electron beam quality control using an amorphous silicon EPID. *Med Phys* 2009; 36:1859-66.
- Mamalui-Hunter M, Li H, Low DA. MLC quality assurance using EPID: a fitting technique with subpixel precision. *Med Phys* 2008;35:2347-55.
- Simon TA, Kahler D, Simon WE, Fox C, Li J, Palta J, *et al*. An MLC calibration method using a detector array. *Med Phys* 2009; 36:4495-503.
- Mohammadi M, Bezak E. Evaluation of MLC leaf positioning using a scanning liquid ionization chamber EPID. *Phys Med Biol* 2007;52:N21-33.
- Mohammadi M, Bezak E, Reich P. Verification of dose delivery for a prostate sIMRT treatment using a SLIC-EPID. *Appl Radiat Isot*



- 2008;66:1930-8.
39. Reich PD, Bezak E. The use of a treatment planning system to investigate the potential for transmission dosimetry in detecting patient breathing during breast 3D CRT. *Australas Phys Eng Sci Med* 2008;31:110-21.
  40. Reich P. A theoretical evaluation of transmission dosimetry in 3D conformal radiotherapy. PhD thesis School of Chemistry and Physics, The University of Adelaide, 2006
  41. Mohammadi M, Bezak E. The physical characteristics of a SLIC-EPID for transmitted dosimetry. *Iran J Radiat Res* 2005;2:175-183.
  42. Mohammadi M, Bezak E. Two-dimensional transmitted dose measurements using a scanning liquid ionization chamber EPID. *Phys Med Biol* 2006;51:2971-85.
  43. Mohammadi M, Bezak E, Reich P. Comparison of two-dimensional transmitted dose maps: evaluation of existing algorithms. *Australas Phys Eng Sci Med* 2006;29:179-87.
  44. Mohammadi M, Bezak E, Reich P. The use of extended dose range film for dosimetric calibration of a scanning liquid-filled ionization chamber electronic portal imaging device. *J Appl Clin Med Phys* 2007;8:69-84.
  45. Low DA, Harms WB, Mutic S, Prudy JA. A technique for the quantitative evaluation of dose distribution. *Med Phys*. 1998; 25:656-661.
  46. van Herk M. Physical aspects of a liquid-filled ionization chamber with pulsed polarizing voltage. *Med Phys* 1991;18:692-702.
  47. van Herk M, Bijhold J, Hoogervorst B, Meertens H. Sampling methods for a matrix ionization chamber system. *Med Phys* 1992;19:409-18.
  48. Dogan N, Leybovich LB, Sethi A. Comparative evaluation of Kodak EDR2 and XV2 films for verification of intensity modulated radiation therapy. *Phys Med Biol* 2002;47:4121-30.
  49. Boellaard R, van Herk M, Mijneer BJ. The dose response relationship of a liquid-filled electronic imaging device. *Med Phys*. 1996; 23:1601-11.
  50. van Herk M, Meertens H. A Matrix ionization chamber imaging device for on-line patient setup verification during radiotherapy. *Radiother Oncol*. 1988;11:369-378.
  51. Varian-medical-system, Portal Vision LC250 MKII. 2000, Palo Alto CA.
  52. Ahnesjo A. Collapsed cone convolution of radiant energy for photon dose calculation in heterogeneous media. *Med Phys* 1989;16:577-92.
  53. Mackie TR, Scrimger JW, Battista JJ. A convolution method of calculating dose for 15-MV x rays. *Med Phys* 1985;12:188-96.
  54. Battista JJ, Sharpe MB. True three-dimensional dose computations for megavoltage X-ray therapy: a role for the superposition principle. *Australas Phys Eng Sci Med* 1992;15:159-78.

**How to cite this article:** Mohammadi M, Bezak E. Evaluation of relative transmitted dose for a step and shoot head and neck intensity modulated radiation therapy using a scanning liquid ionization chamber electronic portal imaging device. *J Med Phys* 2012;37:14-26.  
**Source of Support:** Nil, **Conflict of Interest:** None declared.